

Supporting Information

Doping hafnium with high ligand field to modulate electronic structure of Fe/NC achieving remarkable activity for ORR in Zn-air and Mg-air batteries

Jili Ren, Min Wang, Feng Fu, Zhenjiang Lu*, Jing Xie, Jindou Hu, Yali Cao*

State Key Laboratory of Chemistry and Utilization of Carbon Based Energy Resources,
College of Chemistry, Xinjiang University, Urumqi 830017, Xinjiang, PR China.

*Corresponding authors.

Email: caoyali523@163.com (Y.L. Cao); luzhenjiang318@126.com (Z.J. Lu).

S1 Experimental section

S1.1 Reagents

2-Methylimidazole ($C_4H_6N_2$, AR, 98%), zinc nitrate hexahydrate ($Zn(NO_3)_2 \cdot 6H_2O$, AR, 98.5%), potassium hydroxide (KOH, AR, 98.5%) and hafnium(IV) chloride ($HfCl_4$, AR, 99.5%), were obtained from Aladdin. Iron nitrate nonahydrate ($Fe(NO_3)_3 \cdot 9H_2O$, AR, 98.5%) was gained from Chengdu Kelong Chemical Co., Ltd. Methanol (CH_4O , AR, 99.5%), isopropanol (C_3H_8O , AR, 99.7%), and sodium chloride (NaCl, AR, 99.5%) were acquired from Tianjin Zhiyuan Chemical Reagent Co., Ltd. Commercial platinum carbon (Pt/C, AR, 20%) was purchased from Suzhou Yilongsheng Energy Technology Co., Ltd. Nafion (5 wt%) was bought from DuPont Corporation.

S1.2 Materials characterization

The phase and composition of the synthesized samples were analyzed by X-ray powder diffraction (XRD, Bruker D8 Advance, Germany) with Cu-K α radiation of 0.154 nm wavelength. The analysis was performed to determine the phase and composition of the synthesized samples. Field emission scanning electron microscopy (FESEM, ZEISS Sigma 300, Germany) was used to detect the surface morphology of the samples. The internal hyperfine structure and elemental distribution of the samples were systematically characterized using transmission electron microscopy (TEM, FEI-TALOS-F200X, USA), high-resolution TEM (HRTEM, FEI-TALOS-F200X, USA), and energy dispersive X-ray spectroscopy (EDS, FEI-TALOS-F200X, USA). The degree of graphitization and defect characteristics of the samples were systematically characterized and analyzed using confocal Raman spectroscopy (Raman, HORIBA HR Evolution, France) with an excitation wavelength of 532 nm. The elemental composition and valence states on the surface of the samples were analyzed using Al-K α X-ray photoelectron spectroscopy (XPS, Thermo Scientific K-Alpha, USA). The contents of Hf and Fe elements in the samples were quantitatively analyzed by inductively coupled plasma atomic emission spectrometer (ICP-OES, PerkinElmer Optima 8000, USA).

S1.3 Oxygen reduction reaction (ORR) tests

Before the test, continuously introduce nitrogen or oxygen into the electrolyte for 0.5 hours to ensure that the electrolyte reaches a saturated state with nitrogen or oxygen. Subsequently, cyclic voltammetry tests were conducted for 10 cycles at a scan rate of 100 mV s⁻¹ within the potential window of -1 to 0.2 V. Within the same voltage window, polarization curves (linear sweep voltammetry) tests were carried out at a scan rate of 10 mV s⁻¹ and a rotation speed of 1600 rpm. The Tafel slope was obtained from the LSV plot using a linear fit applied to points in the Tafel region. The electrochemical impedance spectrum (EIS) of the sample is tested at a current density of 10 mA cm⁻² in the frequency range of 0.01 to 100 KHz. In order to study the kinetics of ORR, LSV curves were collected in oxygen saturated solutions at different rotational speeds (400, 625, 900, 1225, 1600, and 2025 rpm). The kinetic-limiting current density (j_K) for the ORR was derived from the experimental data using the Koutecky-Levich equation and the collected LSV curves are processed to obtain the Koutecky Levich plot (K-L curve). The K-L equation is specified as follows:

$$j^{-1} = j_K^{-1} + j_L^{-1} = j_K^{-1} + (B\omega^{\frac{1}{2}})^{-1} \quad (S1)$$

$$B = 0.2 n F C_0 (D_0)^{\frac{2}{3}} \nu^{-\frac{1}{6}} \quad (S2)$$

where j and j_L are the measured current and diffusion limiting current, respectively; B is the slope of the K-L equation, ω is the rotation speed in rpm, F is the Faraday constant (96,485 C mol⁻¹), n is the number of electron transfers per oxygen molecule, C_0 is the bulk concentration of oxygen (1.2×10^{-6} mol cm⁻³), D_0 is the diffusion coefficient of oxygen in 0.1 M KOH (1.9×10^{-5} cm² s⁻¹), and ν is the dynamic viscosity of the electrolyte (0.01 cm² s⁻¹).

When using RRDE testing, a dual working electrode mode is applied to collect ring current and disk current. The RRDE test is conducted at 1600 rpm, hydrogen peroxide yield ($H_2O_2\%$) and electron transfer number (n) are determined via the following equation:

$$n = 4 j_D / [j_D + (j_R/N)] \quad (S3)$$

$$H_2O_2(\%) = 200 (j_R/N) / [j_R/(N + j_D)] \quad (S4)$$

Where j_D is the disk current, j_R is the ring current, and $N = 0.37$ is the current collection

efficiency of Pt ring.

Commercial Pt/C was selected as the benchmark catalyst. The methanol tolerance of Hf-Fe/NC was further investigated by chronopotentiometry. At a voltage of - 0.37 V and a rotation speed of 1600 rpm, 3 mL methanol solution was added to the electrolyte, and the current changes were observed. According to the Nernst equation $E_{(RHE)} = E_{(Hg/HgO)} + 0.059 \times pH + 0.098$, the potentials reported in this paper have been calibrated to the reversible hydrogen electrode (RHE). Finally, the stability of the oxygen reduction reaction of Hf-Fe/NC and commercial Pt/C catalysts was measured also by chronopotentiometry.

S1.4 Rechargeable Zn-air batteries (ZABs)

ZABs were assembled with polished zinc plates as the anode, carbon paper coated with a catalyst as the air cathode, and a mixed solution of 6 M KOH and 0.2 M Zn(OAc)₂ as the electrolyte. To enhance long-term cycling stability and prevent electrolyte leakage in water-based ZABs, a gas diffusion layer was added on the air cathode side. For comparison, the benchmark catalyst (Pt/C) was assembled on the air cathode. The open circuit voltage, polarization curve and specific capacity of the Zn-air battery were tested on the CHI760E electrochemical workstation. To evaluate its rate performance, constant current discharge tests were conducted at different current densities (1 mA cm⁻², 5 mA cm⁻², 10 mA cm⁻², 20 mA cm⁻², 30 mA cm⁻², and 50 mA cm⁻²). Cycling stability testing of batteries were conducted on the LAND CT2001A system. The cyclic constant current pulse method was used to collect the cyclic curve using a current density of 5 mA cm⁻², and a charging/discharging time of 10 min.

S1.5 Rechargeable Mg-air batteries (MABs)

MABs were assembled using the polished Mg plate as anode, carbon paper coated with catalyst as air cathode, and a mixture of 3.5 Wt% NaCl as electrolyte. As a comparison, the business catalyst (Pt/C) was assembled on an air cathode. The open-circuit voltage, polarization curve, and specific capacity of the Zn-air battery were evaluated using the CHI760E electrochemical workstation, and constant current discharge tests were conducted at different current densities (1 mA cm⁻², 5 mA cm⁻², 10 mA cm⁻², 20 mA cm⁻², and 30 mA cm⁻²) to evaluate its rate performance.

S2 Supplementary Figures and Tables

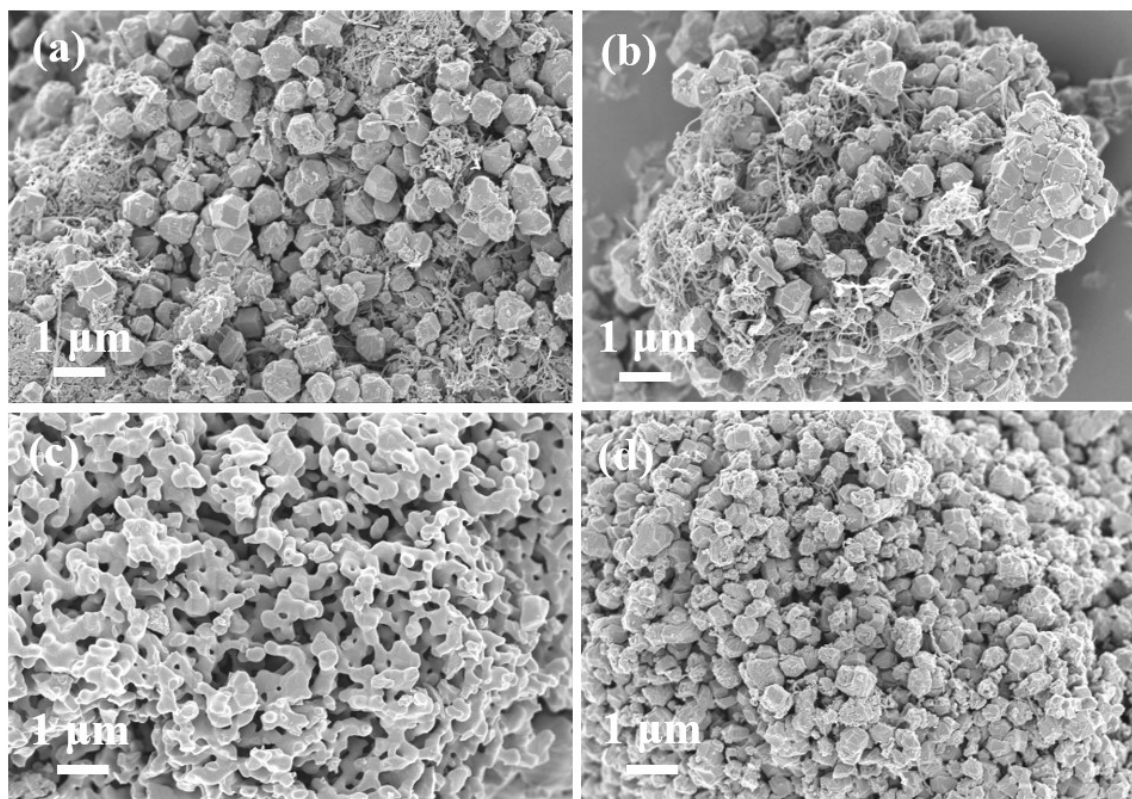


Fig. S1. FESEM images of (a,b) Hf-Fe/NC, (c) Hf/NC, and (d) Fe/NC.

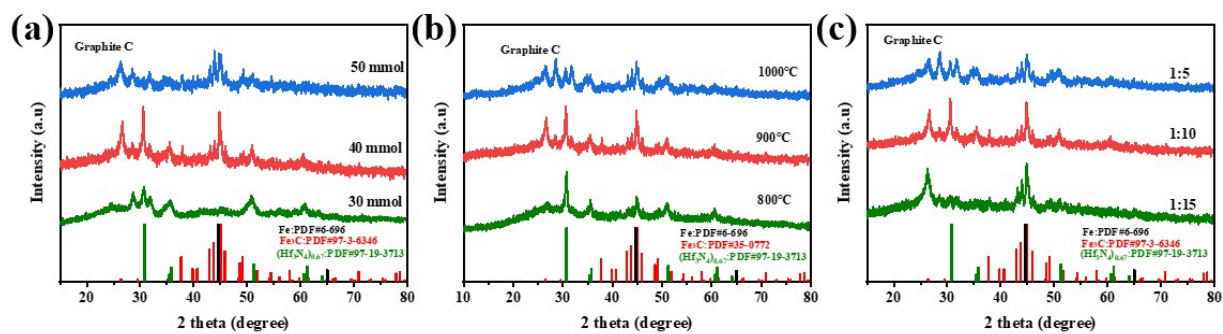


Fig. S2. XRD patterns of samples prepared under different conditions of (a) N doping amounts, (b) temperatures, and (c) Hf:Fe molar ratios.

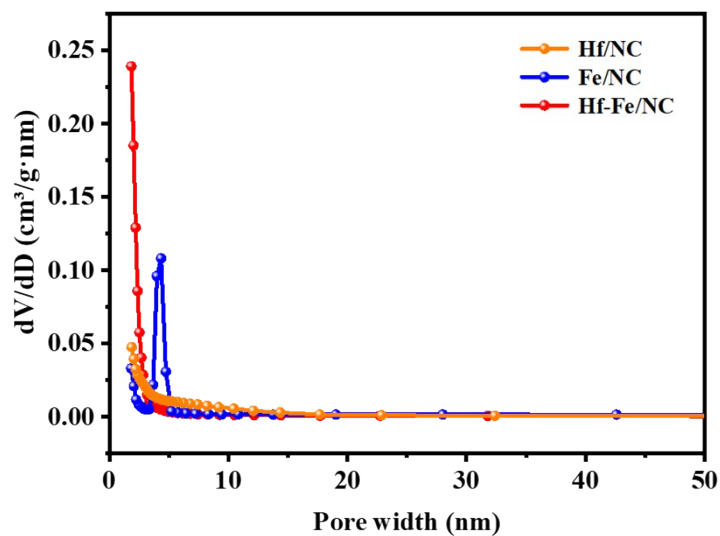


Fig. S3. the curves of BJH pore size distribution for Hf/NC, Fe/NC and Hf-Fe/NC.

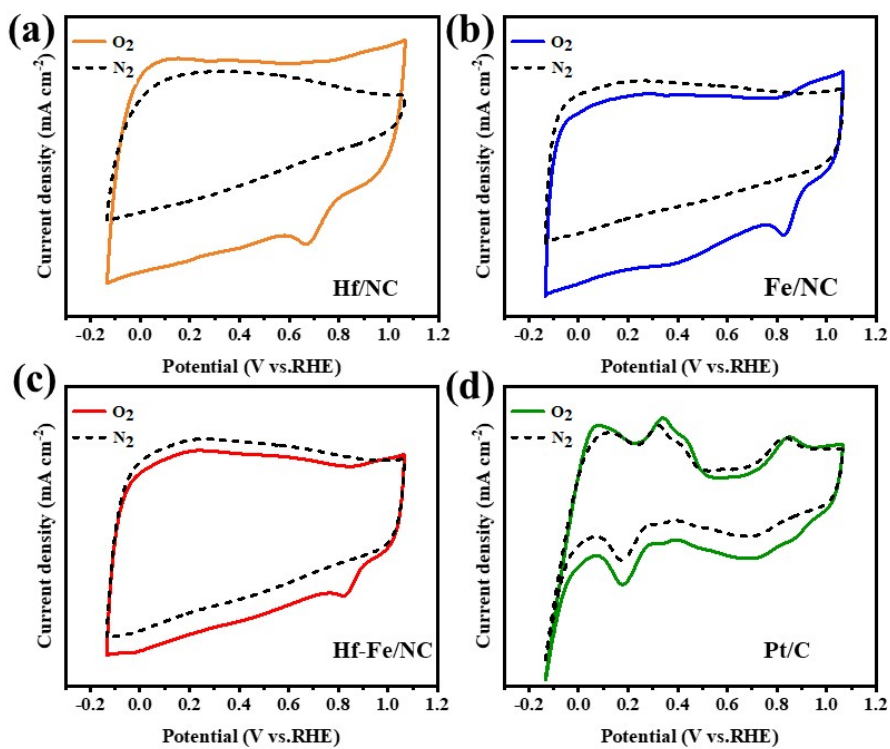


Fig. S4. CV curves of ORR in the O_2/N_2 -saturated 0.1 M KOH.

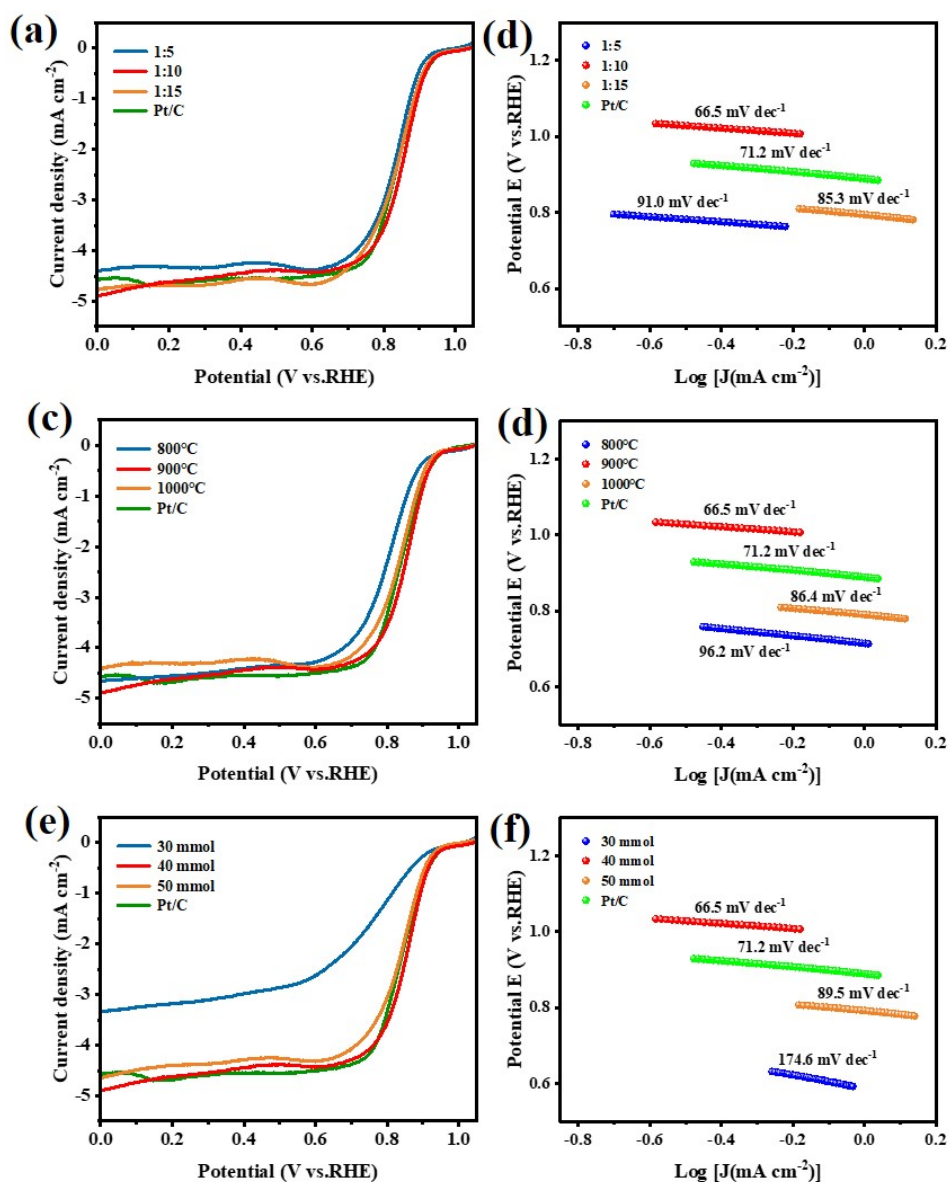


Fig. S5. LSV curves of ORR in the O_2 -saturated 0.1 M KOH and corresponding Tafel plots for samples prepared under different condition of (a, b) Hf:Fe molar ratios, (c, d) temperatures, and (e, f) N doping amounts.

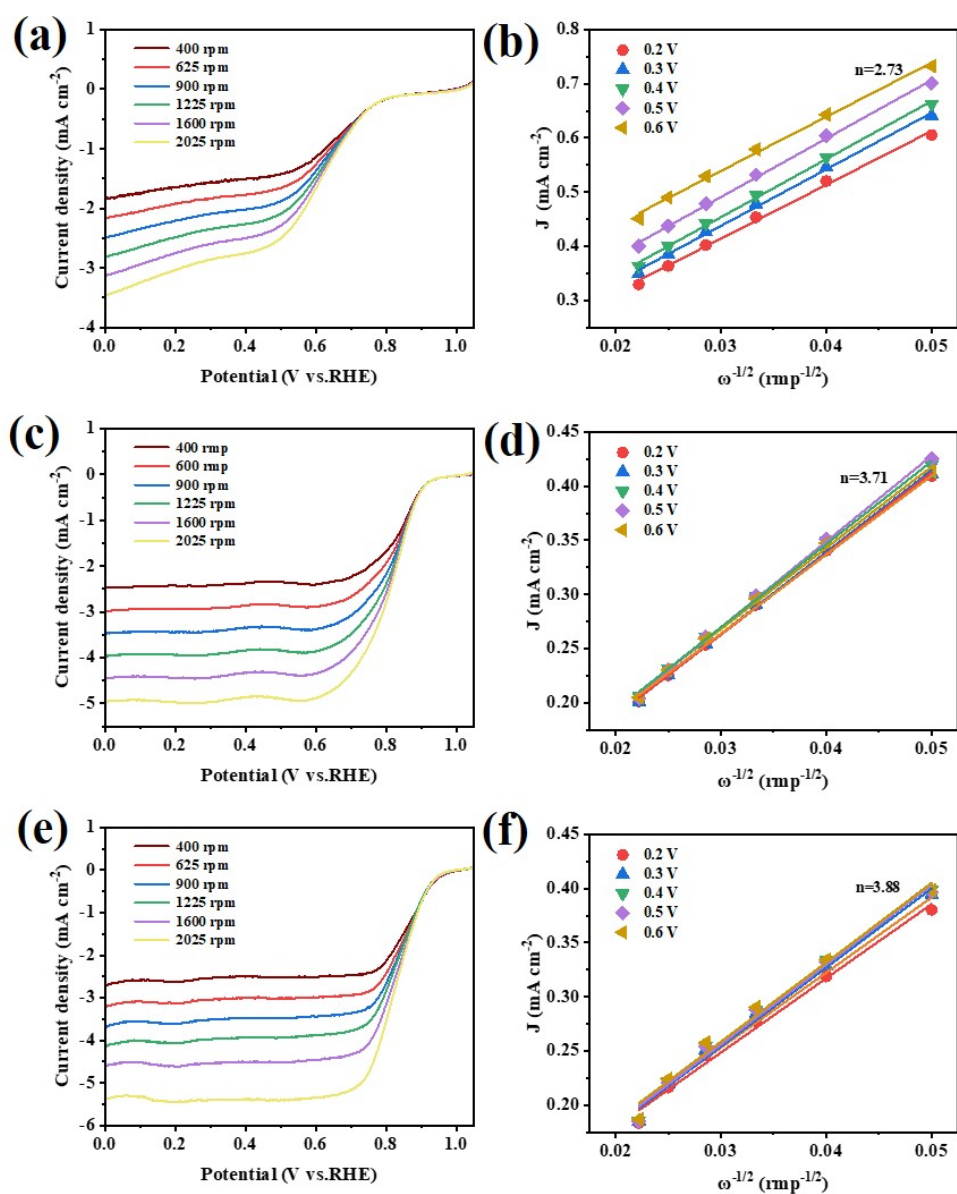


Fig. S6. LSV curves at different rotating speeds in an O_2 -saturated 0.1 M KOH solution of (a) Hf/NC, (c) Fe/NC, and (e) commercial Pt/C, the corresponding Koutecky-Levich (K-L) plots of j^{-1} vs $\omega^{-1/2}$ at different potentials derived from the RDE data of (b) Hf/NC, (d) Fe/NC, and (f) commercial Pt/C.

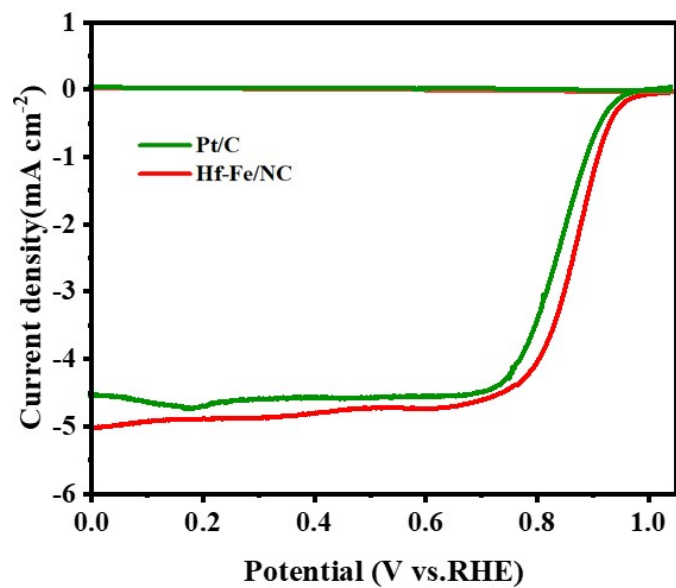


Fig. S7. RRDE measurement at 1600 rpm.

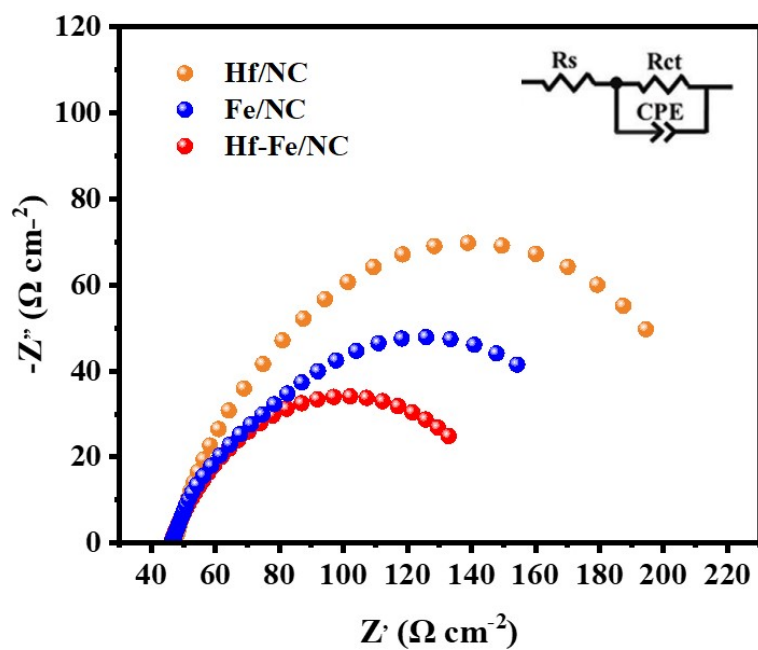


Fig. S8. EIS measurement for Hf/NC, Fe/NC, and Hf-Fe/NC.

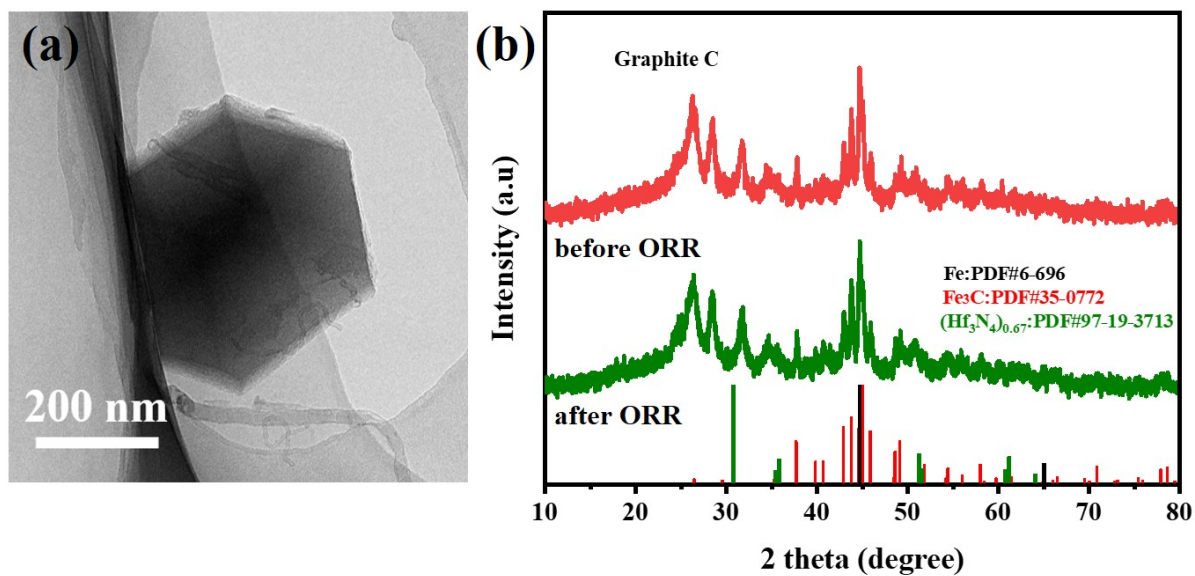


Fig. S9. (a)TEM image, (b)XRD patterns of Hf-Fe/NC after i-t test towards ORR.

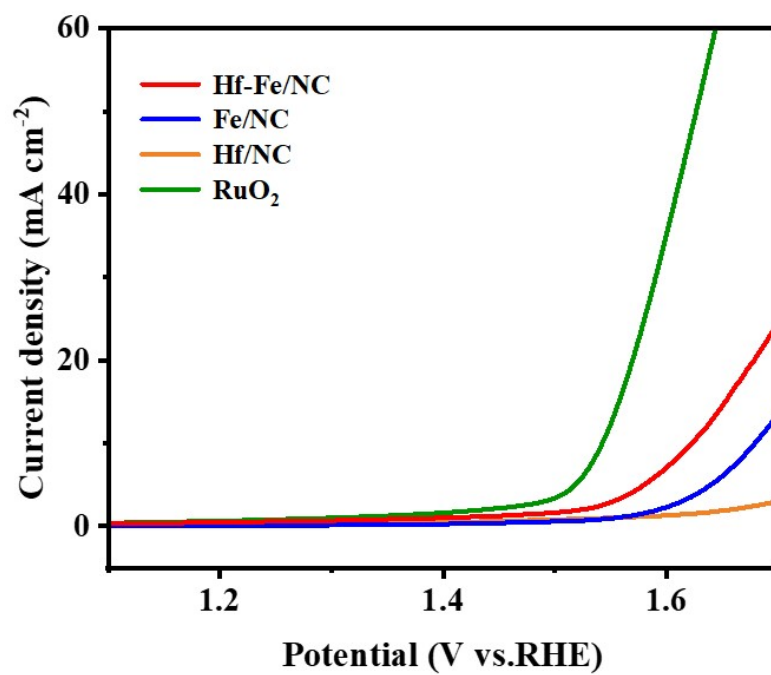


Fig. S10. OER polarization curves of Hf-Fe/NC, Fe/NC, Hf/NC, and commercial RuO₂.

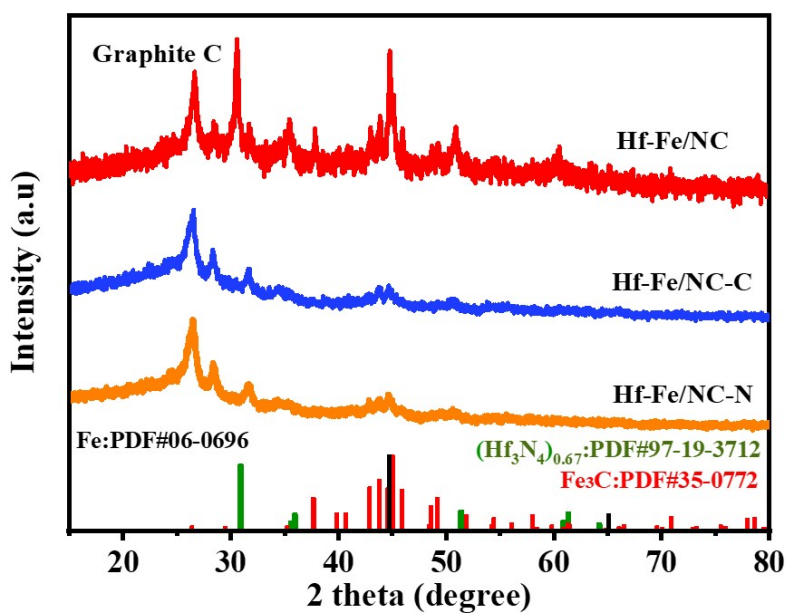


Fig. S11. XRD patterns of Hf-Fe/NC, Hf-Fe/NC-C and Hf-Fe/NC-N.

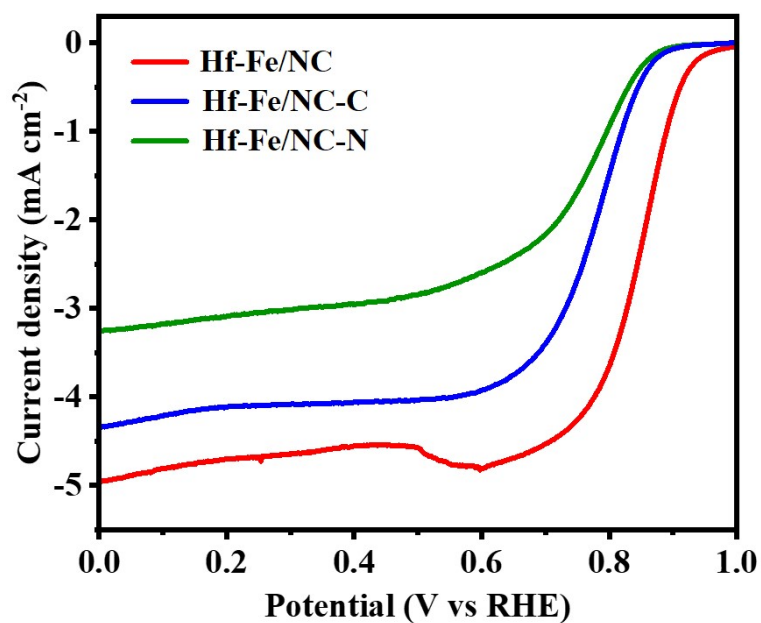


Fig. S12. LSV curves toward ORR in 0.1 M KOH of Hf-Fe/NC, Hf-Fe/NC-C and Hf-Fe/NC-N.

Table S1. The Hafnium and iron ratio in Hf-Fe/NC.

EDS	XPS	ICP
1:11.4	1:9.8	1:8.5

Table S2. ORR activities of the as-synthesized electrocatalysts.

Electrocatalysts	E_{1/2} (V vs RHE)	K_{tafel} (mV dec⁻¹)	Transfer electron number	Reference
Hf-Fe/NC	0.85	66.5	3.99	This work
Pt/C	0.83	78.0	3.88	This work
Fe-Co-NC	0.88	54.8	3.93	[1]
Co-N-P _x -MC	0.84	66	/	[2]
Fe/Mn-N _x -C	0.88	102	~4	[3]
Fe ₂ -S ₁ N ₅ /SNC	0.83	53.6	3.81	[4]
Fe-NiNC-50	0.85	55	3.9	[5]
FeCo-N-C	0.85	41.8	3.82	[6]
Fe ₃ Co-NC@900	0.88	62.1	/	[7]
NPCNF-O	0.85	66	3.9	[8]
NiFe ₂ O ₄ /FeNC	0.83	69	3.87	[9]
FeCoNC/D	0.89	37.2	3.93	[10]
FeNC-V _N	0.90	44	~4	[11]
VP/CNs	0.86	90.0	3.45	[12]
Co@EMPC	0.87	/	3.9	[13]
Fe/Fe ₃ C@CNTs-NWs	0.86	76	3.8	[14]
Co ₃ O ₄ @ND-CN	0.81	64	/	[15]
Mo-Co ₂ P@PNC	0.84	47.8	3.85	[16]

Table S3. The comparative performance of the Hf-Fe/NC based rechargeable ZAB with recently reported state-of-the-art air-cathode based ZAB.

Electrocatalysts	OCP (V)	Power density (mW cm⁻²)	Specific capacity (mA h g_{Zn}⁻¹)	Durability (h) @j (mA cm⁻²)	Reference
Hf-Fe/NC	1.44	160	811@10	300@5	This work
Pt/C	1.39	102	692@10	67@5	This work
FeMn-DSAC	1.45	184	734@2	80@2	[17]
Fe,Zn-N-C	1.45	138	748.6@5	220@5	[18]
PtFeNC	1.49	148	807@10	24@10	[19]
FeCu SACs/NC	1.48	153	741.9@10	/	[20]
Fe-N-C-x	1.47	112	821.8@10	70@10	[21]
Fe-SA/NC	1.52	240	815@5	1050@5	[22]
CNCo-Fe ₃ C	1.47	124	796@20	400@5	[23]
FeCo-MnO@NC	1.46	253	761@10	314@1	[24]
Se/Fe-Co ₃ O ₄ /N-CNs	1.41	141	766@10	/	[25]
Fe-N-C	1.47	175	775.7@10	643@10	[26]
Fe/Cu-N-C	1.50	116	809@10	/	[27]
Co _{0.7} Fe _{0.3} /Fe ₃ C	1.43	249	808@20	124@5	[28]
FeCoNC/D	1.48	157	725@10	40@10	[29]
Fe-Se/NC	1.47	135	764@5	200@20	[30]
Zn,Fe/NC	1.38	170	796@10	500@10	[31]
FeMn-N-C	1.49	151	795@10	700@10	[32]
FeCo-DACs	1.46	158	800@10	500@10	[33]
CNCo-Fe ₃ C	1.47	124	796@5	400@5	[34]

References

- 1 L. Wu, Y. Chen, C. Shao, L. Wang and B. Li, *Adv. Funct. Mater.*, 2024, **34**, 2408257.
- 2 S. Cai, Z. Meng, G. Li, Y. An, Y. Cheng, E. Kan, B. Ouyang, H. Zhang and H. Tang, *Nano Res.*, 2023, **16**, 5887-5893.
- 3 Z. Chen, X. Liao, C. Sun, K. Zhao, D. Ye, J. Li, G. Wu, J. Fang, H. Zhao and J. Zhang, *Appl. Catal. B: Environ. Energy*, 2021, **288**, 120021.
- 4 Y. Li, X. Luo, Z. Wei, F. Zhang, Z. Sun, Z. Deng, Z. Zhan, C. Zhao, Q. Sun, L. Zhang, W. Chen, S. Li and S. Pang, *Energy Environ. Sci.*, 2024, **17**, 4646-4657.
- 5 X. Zhu, D. Zhang, C.J. Chen, Q. Zhang, R.S. Liu, Z. Xia, L. Dai, R. Amal and X.Y. Lu, *Nano Energy*, 2020, **71**, 104597.
- 6 H. Liu, J. Huang, K. Feng, R. Xiong, S. Ma, R. Wang, Q. Fu, M. Rafique, Z. Liu, J. Han, D. Hua, J. Li, J. Zhong, X. Wang, Z. Zhao, T. Yao, S. Jiang, P. Xu, Z. Zhang and B. Song, *Angew. Chem. Int. Ed.*, 2025, **64**, e202419595.
- 7 K. Srinivas, H. Yu, Z. Chen, A. Chen, M. Zhu, Y. Chen and C. Yang, *J. Mater. Chem. A*, 2024, **12**, 16863-16876.
- 8 F. Qiang, J. Feng, H. Wang, J. Yu, J. Shi, M. Huang, Z. Shi, S. Liu, P. Li and L. Dong, *ACS Catal.*, 2022, **12**, 4002-4015.
- 9 Y. Chen, G. Li, L. Hong, Y. Wang, N. Wang, Z. Liu, W.F. Lin and Z. Shi, *ACS Appl. Energy Mater.*, 2023, **6**, 6357-6369.
- 10 K. Kim, K. Min, Y. Go, Y. Lee, S.E. Shim, D. Lim and S.H. Baeck, *Appl. Catal. B: Environ. Energy*, 2022, **315**, 121501.
- 11 L. Lyu, X. Hu, S. Lee, W. Fan, G. Kim, J. Zhang, Z. Zhou and Y.M. Kang, *J. Am. Chem. Soc.*, 2024, **146**, 4803-4813.
- 12 H. Xia, R. Pang, X. Dong, Q. Liu, J. Chen, E. Wang and J. Li, *J. Am. Chem. Soc.*, 2023, **145**, 25695-25704.
- 13 Y. Zhao, L. Zhu, J. Tang, L. Fu, D. Jiang, X. Wei, H. Nara, T. Asahi and Y. Yamauchi, *ACS Nano*, 2023, **18**, 373-382.
- 14 C. Xu, Y. Niu, S. Gong, X. Liu, M. Xu, T. Liu and Z. Chen, *ChemSusChem*, 2022, **15**, e202200312.

- 15 W. Tang, K. Teng, W. Guo, F. Gu, B. Li, R. Qi, R. Liu, Y. Lin, M. Wu and Y. Chen, *Small*, 2022, **18**, 2202194.
- 16 J. Han, J. Zhou, W. Song, H. Zhang, Z. Wang, K. Liu, Y. Li, W. Zhu, X. Sun and H. Liang, *Appl. Catal. B: Environ. Energy*, 2024, **359**, 124468.
- 17 T. Cui, Y.P. Wang, T. Ye, J. Wu, Z. Chen, J. Li, Y. Lei, D. Wang and Y. Li, *Angew. Chem. Int. Ed.*, 2022, **61**, e202115219.
- 18 Y. Yao, T. Jiang, S.Y. Lim, C. Frandsen, Z. Li, Y. Dou, F. Wu, J. Qin, J. Zou, E. Stamate and W. Zhang, *Small*, 2023, **19**, 2304655.
- 19 X. Zhong, S. Ye, J. Tang, Y. Zhu, D. Wu, M. Gu, H. Pan and B. Xu, *Appl. Catal. B: Environ. Energy*, 2021, **286**, 119891.
- 20 H. Liu, L. Jiang, Y. Wang, X. Wang, J. Khan, Y. Zhu, J. Xiao, L. Li and L. Han, *Chem. Eng. J.*, 2023, **452**, 138938.
- 21 X.S. Guo, Z.Y. Huang, X.W. Qi, L.P. Si, H. Zhang and H.Y. Liu, *J. Electroanal. Chem.*, 2023, **936**, 117381.
- 22 L. Yang, Y. Zhu, X. Yao, C. Du, Z. Han, J. Tian, X. Liu, X. Ma and C. Cao, *Energy Storage Mater.*, 2023, **63**, 102972.
- 23 S.S. Li, F.F. Chang, Y. Yuan, K. Zhu, W.T. Chen, Q. Zhang, Z.S. Lu, Z.Y. Bai and L. Yang, *J. Colloid Interface Sci.*, 2023, **651**, 734-741.
- 24 Y. Ye, L. Zhang, Q.L. Zhu, Z. Du, T. Wagberg and G.Z. Hu, *J. Colloid Interface Sci.*, 2023, **650**, 1350-1360.
- 25 H. Zhao, H. Yao, S. Wang, Y. Cao, Z. Lu, J. Xie, J. Hu and A. Hao, *J. Colloid Interface Sci.*, 2022, **626**, 475-485.
- 26 X. Lu, H. Xu, P. Yang, L. Xiao, Y. Li, J. Ma, R. Li, L. Liu, A. Liu, V. Kondratiev, O. Levin, J. Zhang and M. An, *Appl. Catal. B: Environ. Energy*, 2022, **313**, 121454.
- 27 W. Zhang, B. Feng, L. Huang, Y. Liang, J. Chen, X. Li, Z. Shi and N. Wang, *Appl. Catal. B: Environ. Energy*, 2024, **358**, 124450.
- 28 S. Das, A. Pathak, U. Phadikar, C. Kuila, A. Maji, T. Kuila, N.C. Murmu, R. Thapa and A. Kundu, *Adv. Funct. Mater.*, 2024 **34**, 2407078.
- 29 K. Kim, K. Min, Y. Go, Y. Lee, S.E. Shim, D. Lim and S.H. Baeck, *Appl. Catal. B: Environ. Energy*, 2022, **315**, 121501.

- 30 Y. Wang, J. Wu, S. Tang, J. Yang, C. Ye, J. Chen, Y. Lei and D. Wang, *Angew. Chem. Int. Ed.*, 2023, **62**, e202219191.
- 31 M. Ye, J. Wang, L. Zhan, M. Wang, W. Yan, Y. Wang, K. Yang, H. Liu, Y. Tan, W. Wang, C. Chen and K. Wu, *ACS Appl. Energy Mater.*, 2024, **7**, 3061-3070.
- 32 C. Hu, G. Xing, W. Han, Y. Hao, C. Zhang, Y. Zhang, C.H. Kuo, H.Y. Chen, F. Hu, L. Li and S. Peng, *Adv. Mater.*, 2024, **36**, 2405763.
- 33 J. Qiao, Y. You, L. Kong, W. Feng, H. Zhang, H. Huang, C. Li, W. He and Z.M. Sun, *Adv. Mater.*, 2024, **36**, 2405533.
- 34 S. Li, F. Chang, Y. Yuan, K. Zhu, W. Chen, Q. Zhang, Z. Lu, Z. Bai and L. Yang, *J. Colloid Interf. Sci.*, 2023, **651**, 734-741.